PROCEEDINGS, 43rd Workshop on Geothermal Reservoir Engineering
Stanford University, Stanford, California, February 12-14, 2018
SGP-TR-213

Constraining of Focal Mechanisms of Induced Seismicity Using Borehole Logging Information

Yusuke Mukuhira, Kazumasa Fuse, Makoto Naoi, Michael Fehler, Takatoshi Ito, Hirokazu Moriya, Hiroshi Asanuma, Markus O. Häring

MIT Earth Resources Laboratory, 77 Massachusetts Avenue Cambridge, MA 02139-4307

mukuhira@mit.edu

Keywords: induced seismicity, focal mechanism, borehole logging, in-situ stress, existing fracture

ABSTRACT

Monitoring of microseismicity is essential for successful hydraulic stimulation in Enhanced/Engineered geothermal development. Hypocenter locations of the microseismic events are indicators of fractures whose permeability has been enhanced by shear slip. In addition to the locations of microseismic events, knowledge about the geometry of the fracture network is also important for better understanding of the fractured reservoir, flow, and design of the heat extraction system since fracture geometry is directly correlated to permeability. Focal mechanisms contain first order information about the fracture network. However, due to the small number of monitoring stations in geothermal microseismic monitoring, it is often difficult to constrain the focal mechanisms of microseismicity from first motion information. We propose a novel method to overcome this limitation and estimate focal mechanism by including borehole logging information such as *in-situ* stress and information about existing fractures. We estimate the range of fault planes which can have shear slip in a given stress state and increase of pore pressure. By referring to that range, we eliminate candidate of focal mechanisms which are consistent with first motion information but not consistent with *in-situ* stress. As another approach, we use existing fracture information from borehole logging. We establish a statistical model of existing fractures and calculate the likelihood of shear slip from all candidate focal mechanisms. By referring to this model, we can reject less unlikely focal mechanisms and chose more likely ones. Thus, we can constrain the focal mechanisms considering not only seismological information but also other geophysical information. We apply our method to field data from Basel, Switzerland and examine the performance and the feasibility of our method by comparing with the well constrained focal mechanisms of larger events determined using data from a regional network.

1. INTRODUCTION

In the field of Enhanced/Engineered Geothermal System(EGS) development and conventional geothermal system, microseismicity is often used as an essential real time reservoir monitoring method. Especially in the case of EGS with hydraulic stimulation, microseismicity is induced by increase of pore pressure and the presence of induced seismicity is a direct indicator of permeability enhancement. Locations of microseismic events provide the position of the fractures whose permeability is enhanced by opening or shear slip. Measurement of microseismicity is thus important for evaluating the effect of the hydraulic stimulation and the shape of the EGS reservoir in real time. In addition to the location of the series of microseismic events, the orientation of the fracture on which microseismicity occurs is also very important since permeability of the stimulated fracture is influenced by the stress state (Ito and Zoback, 2000). Fracture orientation information also is beneficial for understanding the geometry of the fracture system, fluid flow and for designing sustainable and economical plan for energy extraction from the reservoir.

Orientation of the faults on which earthquakes occur (focal mechanism) is often estimated from *P*-wave first motion information which produces what is often referred to as beach ball plot. In general, the a greater the number of first motion measurements i.e. stations, the more precise is the resulting focal mechanism determination. In the geothermal microseismic monitoring situation, it is rare that enough number of monitoring stations are deployed to constrain the focal mechanism precisely. This is because, the primary objective of microseismic monitoring is the precise determination of hypocenter location of microseismicity and there is reluctance to increase the cost for installation of more stations required for reliable focal mechanism determination. Recently, some effort on microseismic monitoring has been undertaken for improvement such as surface monitoring array or use of downhole arrays, but surface monitoring stations usually cannot detect small events and a single downhole array may not cover large enough part of focal sphere to determine the focal mechanism. Therefore, there is a challenge for constraining focal mechanisms of injection induced seismicity under poor (e.g. realistic) monitoring scenarios.

There have been several attempts to constrain focal mechanisms by combining first motion information of *P*-waves and trace amplitude information such as the S/P amplitude ratio (Hardebeck and Shearer, 2003; Kraft *et al.*, 2006). These methods cannot avoid the influence on the waveforms introduced along the path from the source to station. Especially for microseismic events, the uncertainty may critically affect the amplitude due to low signal to noise ration of smaller events, and lead a poor result. So, we take a different approach to constrain the focal mechanism estimated from only several first motion measurements. We propose the novel method to constrain focal mechanism of injection induced seismicity by introducing other geophysical constraints from borehole logging information. In this paper, we focus on the introduction of *in-situ* stress and injection pressure information.

2. CONCEPT

2.1 Concept

When focal mechanisms are estimated using *P*-wave first motions using a grid-search method (Reasenberg and Oppenheimer, 1985), all possible combination of strike, dip and rake are tested to determine if a given focal mechanism defined by three parameters fits observations of first motion. The number of the *P*-wave first motions that are not consistent with a candidate focal mechanism is used as the misfit function. When there are a small number of stations giving poor coverage on the focal sphere, there will be many candidate focal mechanisms stratifying *P*-wave first motion and the focal mechanism is not well constrained (Figure 1a). All candidate focal mechanisms are equally plausible based on the seismic data. The idea of the method we propose is to constrain possible focal mechanism solutions by introducing other geophysical data which are independent of seismic waveform data. In this study, we combine *in-situ* stress data obtained from borehole logging with injection pressure information.

2.2 Introducing *in-situ* stress information

Injection induced seismicity is caused by reduction of normal stress due to pore pressure increase accompanying hydraulic stimulation. When the magnitude and orientation of three principle stresses are given, we can constrain the range of orientations of faults that can have shear slip with a given injection pressure (Ito and Hayashi, 2003). With the *in-situ* stress information, shear and normal stress working on an arbitrary fault can be computed (Zoback, 2007) and then, pore pressure increase necessary for shear slip (ΔP) can also be computed with Coulomb failure criterion of equation (1) a assuming constant friction coefficient.

$$\tau = \mu(\sigma_n - (P_h + P_c)) \tag{1}$$

Figure 1b shows a conceptual lower hemisphere plot of ΔP for poles to arbitrary faults and the range of the faults that can slip at a given wellhead pressure (WHP) are delineated with red lines. We combine two independent measurements (Figures 1a and 1b) and constrain the possible focal mechanisms by rejecting those which are not consistent with *in-situ* stress and WHP. Then, we only plot the possible focal mechanisms in the blue area in figure 1c survive as candidate focal mechanisms. As we show in the schematic image in Figure 1, our method has potential to constrain the possible focal mechanisms by rejecting many candidates that are not consistent with stress and WHP information. Note: our method is not designed to determine one unique focal mechanism but rather it is designed to constrain the range of focal mechanisms using the complementary information from borehole logging.

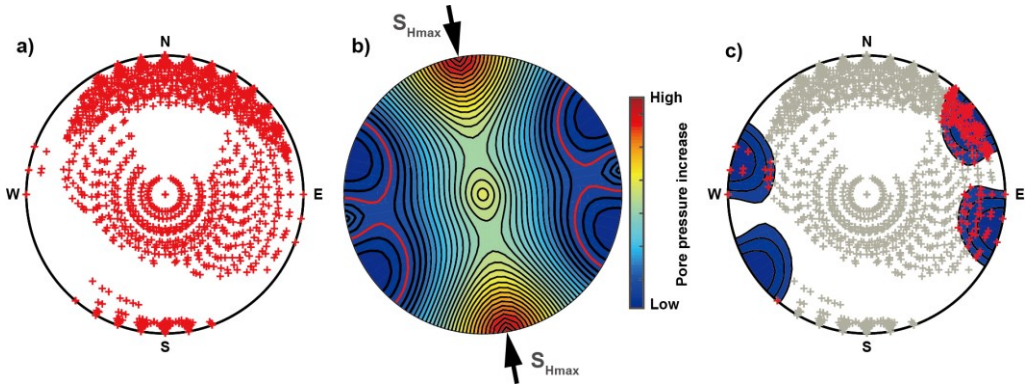

Figure 1: Conceptual image for our proposed method. a) an example of the distribution of poles of all possible fault mechanisms that are consistent with first motion data from a limited number of stations. b) an example of pore pressure increase necessary for shear slip (*ΔP*) under a given stress state. *ΔP* is plotted for poles to arbitrary faults on a lower hemisphere projection. c) Combination of a) possible focal mechanisms from first motion information and b) *in-situ* stress and WHP information. Red crosses plotted in the blue region are candidate of true focal mechanisms. The gray crosses are rejected due to inconsistency with *in-situ* stress data and injection pressure information.

3. DATA USED IN THIS STUDY

3.1 Microseismic data at Basel, Switzerland

We evaluate the performance of the proposed method using microseismic data recorded at the injection for the Basel, Switzerland EGS project. To verify the feasibility of the proposed method, we need the *in-situ* stress information that is obtained independently of the focal mechanisms. In addition to this, we also need reliable focal mechanisms that are estimated by some independent method to use as benchmark focal mechanisms to compare with the results obtained using our method. Several events with relatively large magnitudes were recorded by surface seismic monitoring stations across Switzerland as well as at the local microseismic monitoring stations, and their focal mechanisms were well determined using first motions (Deichmann and Giardini, 2009). Therefore, the Basel EGS data are suitable for our purposes.

The Basel EGS project was operated by Geothermal Explorers Ltd. (GEL, present Geo Explorers Ltd.). A total 11,500 m^3 of water from the Rhine River were injected into several cataclastic fracture zones that intersected the open-hole section (4603–5000 m) of the hole (Häring *et al.*, 2008). Maximum WHP reached 29.6 MPa at a maximum flow rate of 3300 L/min. GEL deployed six borehole stations

each having a 3-component geophone (figure. 2a). The granite basement formation begins at 2265 m (TVD) and above that are several sedimentary formations (Häring *et al.*, 2008). The deepest station (OT2) was located at the top of the granite section; others were in the sedimentary formation. A lower hemisphere projection of the location of these six stations from the top of the open-hole section is shown in figure. 2b. Take off angles from an imaginary source position at the top of open-hole section were estimated by ray tracing through the velocity model. The lower hemisphere projection (figure. 2b) shows that stations had good azimuthal coverage but coverage in the inclination direction was limited, and that means that constraints on focal mechanisms from network first motion data will be poor.

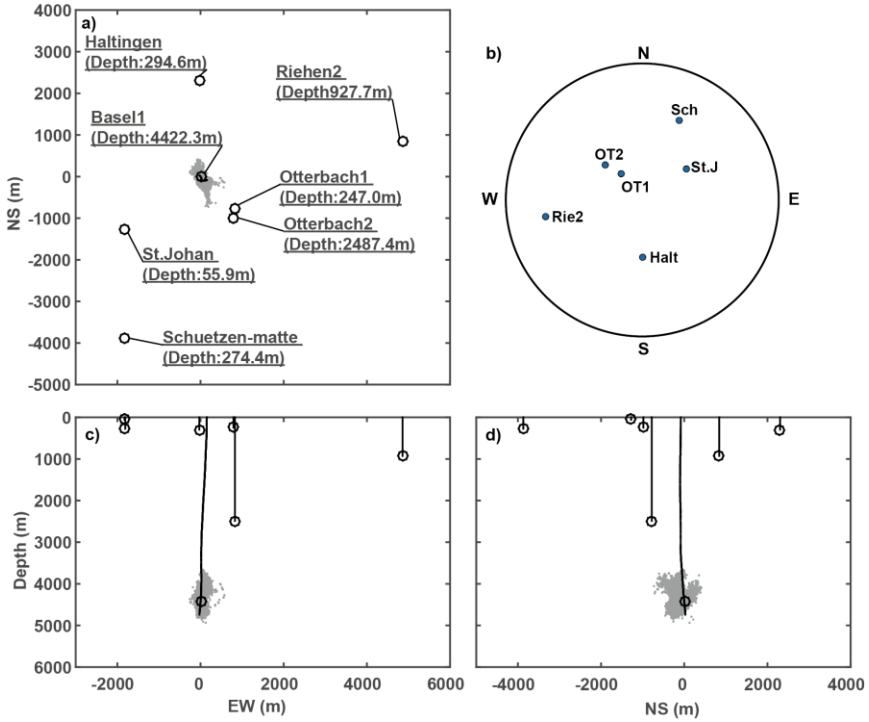

Figure. 2: Microseismic network at Basel with microseismic cloud (gray zone) determined by Asanuma et al., (2008). a) Plan view. b) Lower hemisphere projection of microseismic station locations using the top of the injection zone as a source position. c) EW cross sectional view of stations and locations. d) NS cross sectional view. Note: depth is in TVD relative to surface elevation.

Approximately 13,000 seismic events were recorded by the microseismic network during and after stimulation. Locations were determined using the calibrated 1D velocity model having V_p=3980 and V_s=2080 m/s for the sedimentary layer and V_p=5940 and V_s=3450 m/s for the granite section (Dyer *et al.*, 2008; Häring *et al.*, 2008). GEL determined the hypocenters for around 2700 of the events in real time through February 2007. Subsequently, Asanuma *et al*. (2008) relocated several events by applying the multiplet analysis method (Moriya *et al.*, 2003) and the Double Difference (DD) method (Waldhauser and Ellsworth, 2000). We use hypocenter locations determined by Asanuma *et al*. (2008).

The Swiss Seismological Service (SED) also recorded several events that were sufficiently strong to be well recorded at their surface stations across the country and the Basel downhole microseismic network (Deichmann and Giardini, 2009). Using first motion data from these stations, robust focal mechanisms of 28 of the strongest events were determined (Deichmann and Giardini, 2009). Later, focal mechanisms of additional events were determined (Terakawa *et al.*, 2012), resulting in a total of 118 well constrained focal mechanisms. We choose the events that occurred from the start of stimulation to before shut-in. After shut-in, WHP is not effective as a physical constraint on focal mechanisms. We selected 52 target events out of 118 events for our study. The focal mechanisms of the events are plotted as lower-hemisphere beach balls on a plot of event depth *vs.* occurrence time in Figure 3 with hydraulic record.

3.1.2 *In-situ* stress information

Valley and Evans, (2009) reported that orientation of the maximum horizontal stress (S_{Hmax}), within the granite section at Basel was N144◦E±14◦ from the analysis of borehole breakouts and drilling-induced tensile fractures in the injection well (Basel-1) and the deepest monitoring well (OT2). Valley and Evans (2015) reported stress magnitude inferred from borehole breakout width analysis. Summarized stress estimates are given by

$$S_{Hmax} = 0.00104z + 115 \quad (2)$$

$$S_{hmin} = 0.01990z - 17.78 \quad (3)$$

$$S_v = 0.0249z \tag{4}$$

$$P_h = 0.00981z \tag{5}$$

where S_{Hmax} is maximum horizontal stress, S_{hmin} is maximum horizontal stress, S_v is vertical stress, P_h is hydrostatic pressure, and z is depth respectively. Units for all parameters here are MPa. Due to the small gradient of S_{Hmax} and increasing S_v with depth. the stress state transitions from strike slip to normal faulting at around 4800 m depth. This stress state is consistent with the observation that several large events have normal fault mechanism (Deichmann and Giardini, 2009).

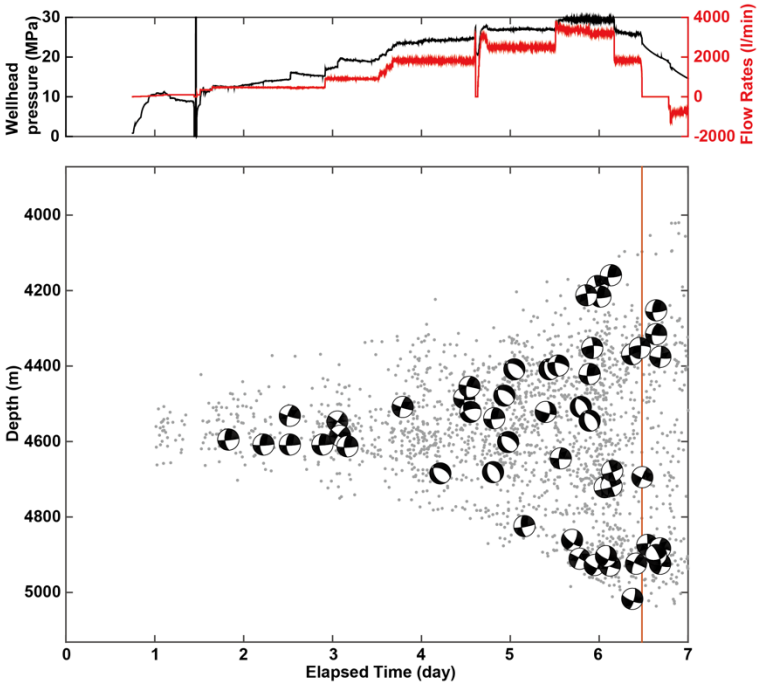

Figure.3: Time series of focal mechanisms and hydraulic record. a) hydraulic record vs. time. Black line: wellhead pressure (WHP). Red line: flow rate. b) Time migration of focal mechanisms of target events vs. depth. Red line indicates the time of shut-in. Gray background dots show locations of other microseismic events.

4. RESULTS AND DISCUSSION

4.1 Procedures

First, we choose events for which the *P*-wave first motions can be read clearly by eye at all 6 microseismic stations. We sorted chosen events into several groups on the basis of patterns of polarities. Since the location of stations on a focal sphere is almost identical for each event, the difference of first motions corresponds to a variation of focal mechanisms assuming double couple source model. Focal mechanisms are estimated by grid-search using 5 degree increments for strike, dip, and rake. We defined those satisfying the first motion information as polarity-consistent focal mechanisms. We can reasonably assume that each member within a group has a nearly identical pole distribution for their polarity-consistent focal mechanisms, because the first motion combinations are identical among the group members and the relative location from source to stations on the focal sphere are almost identical.

For practical implementation, let us introduce original metric "slip index" as follows:

$$slip\ index = \frac{\mathrm{WHP}-\Delta P}{\mathrm{WHP}-\Delta P_{\min}} \qquad (\text{for WHP}>\Delta\text{P}) \tag{1}$$

$$slip\ index = 0 \qquad (\text{for WHP}<\Delta\text{P}) \tag{2}$$

where ΔP is the pore pressure increase required for slip on a given fault. $\Delta P_{\min}$ is the ΔP required for the most optimally-oriented fault. WHP is the wellhead pressure at the occurrence time of the event in consideration. The physical meaning of the slip index is the relative ease with which a given fracture can have shear slip under a given wellhead pressure condition. So, the most well-orientated fault has slip index=1. We assigned faults whose ΔP>WHP slip index=0 to indicate that there is no chance for it to have shear slip. Note that slip index indicates the ease with which shear slip can occur on the fault and the contour of the slip index does not mean the probability or plausibility of the best focal mechanism.

The result of combining first motion and stress data delineates a region of the focal sphere where poles to potential fault planes are consistent with both types of data. This region gives the range where the poles of true focal mechanisms can exist. All polarity-

consistent focal mechanisms that fall in the area of slip index=0 are eliminated. The color contour plots in figures. 4 and 5 show the poles to focal mechanisms that are consistent with both stress and first motion information. To quantitatively evaluate the degree by which *in-situ* stress constrains a focal mechanism, we introduce an index called "elimination rate" which is defined as number of polarity-consistent focal mechanisms that are eliminated by the stress information compared to the total number of polarity-consistent focal mechanisms. High elimination rate means many polarity-consistent focal mechanisms are rejected by introducing *in-situ* stress and WHP information.

For each event, we evaluate the match of our benchmark focal mechanisms determined by SED with the area of non-zero slip index. For the two poles of each benchmark focal mechanism, we search for the closest discretized point used in our grid search and identify whether that point has slip index larger than 0. Mukuhira *et al.*, (2016) identified which focal mechanism plane actually slipped by visual observation of microseismic distribution in the vicinity of each nodal plane of the SED focal mechanisms. Although, we treat the two planes equally but in the following figures, we plot them with different symbols based on the slip plane identified in our previous study.

4.2 Results

We show the result of our method for one particular group as an example. This group has the largest population among all groups. The first motion pattern for this group allows various orientations of possible focal mechanisms as shown in figure 4. After introducing the slip index, many focal mechanisms are eliminated. The results for first event in the group, the one that occurred at the lowest wellhead pressure, is shown in the top right of figure 4. In addition to two regions where slip index peaks along NNE-SSW striking poles, a small area of nonzero slip index exists in the Eastern portion of the focal sphere. One of the poles of the benchmark focal mechanism (diamond marker) is located at the periphery of this area but the other locates outside of nonzero slip index area. All events in this group showed similar tendencies. As WHP increased, the area of high slip index becomes larger, resulting in a decrease of the elimination rate. Despite the high WHP, the events that occurred in the later stage of the stimulation show elimination rates of around 0.6 (figure 6).

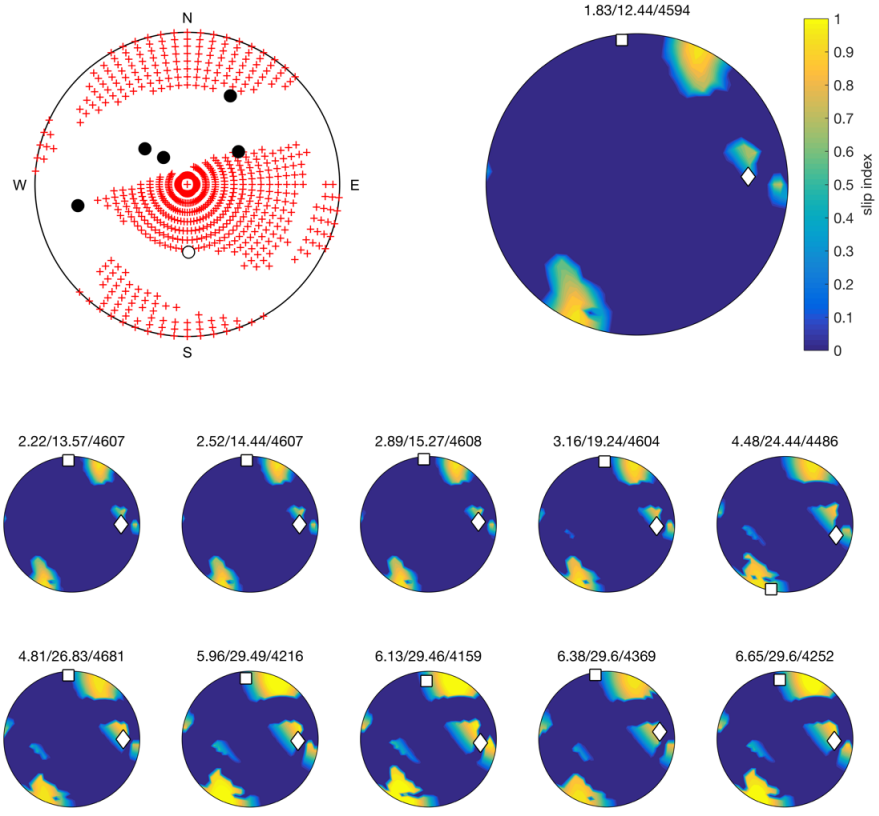

Figure 4: Result of introduction of slip index to constrain polarization-consistent focal mechanisms for events. Upper left panel is lower hemisphere plot of polarity data and poles (red crosses) for all polarity-consistent focal mechanisms . First motion polarities are shown with circles where black means compression and white means dilatation. The color contour plots show the distribution of slip index suggesting the area where the pole of each focal mechanism can exist. Blue areas have slip index 0 and faults with poles in those areas cannot slip. Poles of benchmark focal mechanisms determined by SED are shown with squares and diamonds. The diamond shows the fault estimated as the failure fault plane. The numbers above the contour plots are occurrence time of the event (in hours from the start of injection), WHP at the occurrence time (MPa), and the depth of hypocenter (m), respectively.

As the other example, we show the result for the group which would be identified as normal fault type. Dilatational first motions situated near the center of the focal sphere lead to normal fault type polarity-consistent focal mechanisms (figure 5). The dilatational poles occur on the interior of the focal sphere indicating a moderately dipping fault. They have wide range in azimuth. The poles for polarity-consistent focal mechanisms that fall within a region at the center of the focal square are eliminated by introducing the slip index. Only faults having strikes varying from the orientation of $S_{H\max}$±0~40° are consistent with the stress field. Elimination rate for the first event that occurred under WHP 23.35 MPa is 0.47. Elimination rate does not change drastically with time/WHP as shown in figure 6. The area of nonzero slip index does not change significantly among the events.

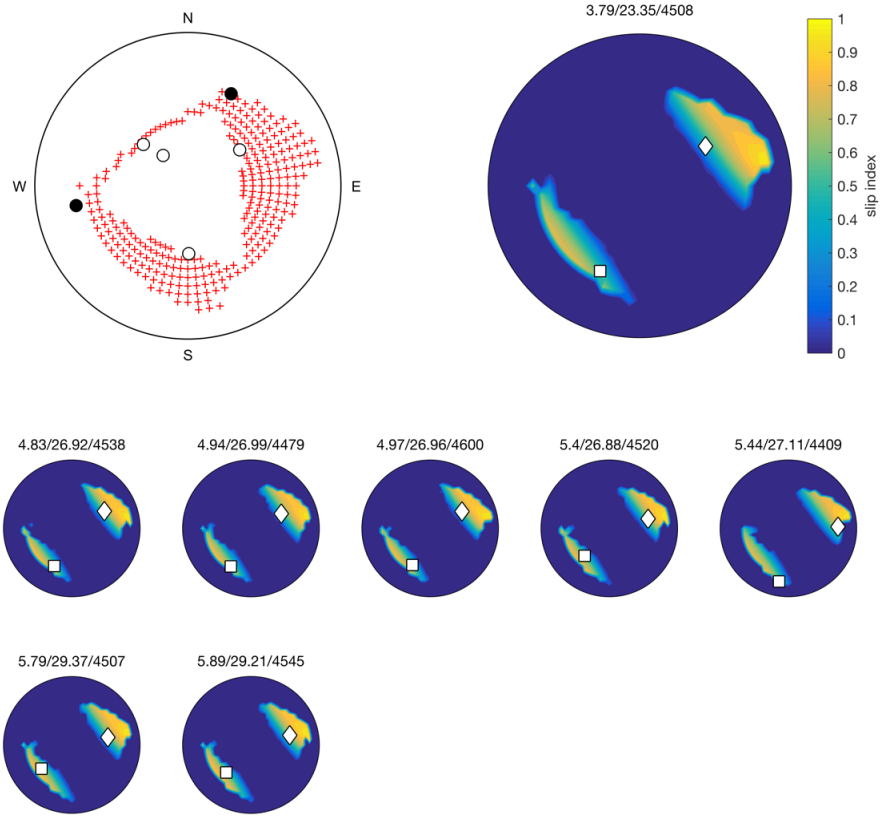

Figure 5: Result of introduction of slip index to possible focal mechanism from first motion for normal fault type Group.

4.3 Discussion

In general, introduction of stress and WHP information successfully constrains the range of focal mechanisms, depending on the distribution of polarity-consistent focal mechanisms. The area of nonzero slip index becomes larger with increasing WHP since high WHP allows faults with a wider range of orientations to slip. Thus, increased WHP is expected to reduce the elimination rate. It also suggests that our method performs very well when WHP is low as we can see in figure 6, in other words, for the events occurring at the initial stage of hydraulic stimulation. We observed that the elimination rate varies significantly between the groups and focal mechanism types. The stress and WHP constraints are particularly useful for cases like the group shown in figure 4, as we observed higher elimination rate (figure 6). The elimination rate decreases significantly with increasing time and WHP which has events at a larger range of occurrence times than the other groups.

The area of nonzero slip index is influenced by the uncertainty in the stress magnitude/orientation and friction coefficient. The uncertainty in elimination rate is simply evaluated by performing a bootstrapping test. The area of nonzero slip index for each event is estimated 1000 times by adding ±10 % normal distribution error on magnitude of horizontal stress and ±14° normal distribution error on orientation of horizontal stress (Valley and Evans, 2009). We exclude all cases where ΔP required for slip are larger than the WHP and where slip-index cannot be defined due to large differential stress. Here, we assume a constant friction coefficient of 0.6 for simplicity. Although, the elimination rate estimated from random tests does not follow a normal distribution, mean value and 95 % confidence level defined two times the standard deviation are shown in figure 6. It seems that the uncertainty tends to be small when elimination rate itself is large and uncertainty is likely to be larger when elimination rate is small. Since the region of the focal sphere with nonzero slip index at low ΔP changes most with perturbation in the stress model, if that region is a small part of the overlapping area between the polarity-consistent focal mechanisms and the nonzero slip index, low uncertainty in elimination rate is expected.

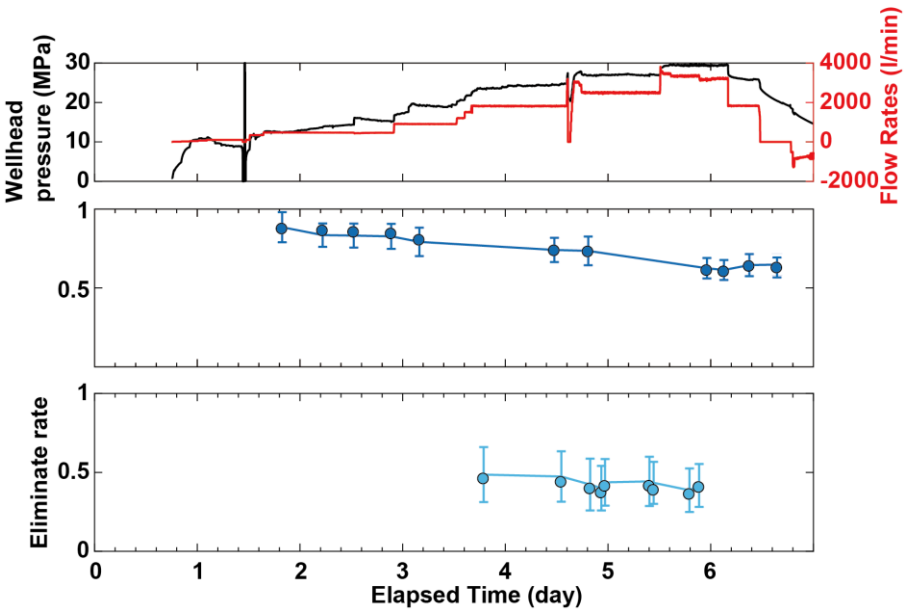

Figure 6: Time series of elimination rate. Circles indicate elimination rate. Error bars for elimination rate are defined using one sigma found using bootstrapping tests. Top panel shows injection flow rate and WHP time series. Second panel shows the result for the group in figure 4 and third panel does for the group in figure 5.

5. CONCLUSION

We have proposed a new method to constrain the range of focal mechanisms of injection induced seismicity determined from small number of first motion data by using *in-situ* stress and injection information. We estimate pore pressure increase required to meet the Coulomb failure criterion for slip along faults with arbitrary orientation. Then by using known WHP information, the range of the faults that could experience failure is determined. Subsequently, the range of the faults estimated from first motion data and those from stress state are superposed, and the focal mechanisms that satisfy both conditions survive as candidates for the true focal mechanism. This is a totally new approach for determining seismological parameters by introducing other geophysical data to complement seismological theory/data.

We applied our method to a microseismic data set collected during a hydraulic injection in Basel Switzerland where stress information and well constrained benchmark focal mechanism data are available. By comparison with the well constrained focal mechanisms, we showed that our proposed method successfully constrained the range of focal mechanisms and we found the constrained region contains the benchmark focal mechanism. Our proposed method provides the greatest constraint on focal mechanism when WHP is low. Even under non-optimal conditions, the range of focal mechanisms was reduced. Consequently, our proposed method demonstrates sufficient feasibility to constrain the focal mechanisms of injection induced seismicity where focal mechanism is not often reliably determined because of poor coverage of polarity data resulting from a small number of stations.

ACKNOWLEDGEMENT

We thank Geo Explorers Ltd. and Geo-Energie Suisse AG for providing the microseismic wave data sets and for permission to publish the results. This study was supported by Grant-in Aid for JSPS Overseas Research Fellow (20160228) and ERL, MIT.

REFERENCES

Asanuma, H., Kumano, Y., Hotta, A., Niitsuma, H., Schanz, U., and Häring, M.: Analysis of microseismic events from a stimulation at Basel, Switzerland, *GRC Transactions*, **31**, (2007), 265–270.

Deichmann, N. and Giardini, D.: Earthquakes Induced by the Stimulation of an Enhanced Geothermal System below Basel (Switzerland), *Seismological Research Letters*, **80**, (2009), 784–798.

Dyer, B. C., Schanz, U., Ladner, F., Häring, M. O. and Spillman, T.: Microseismic imaging of a geothermal reservoir stimulation, *The Leading Edge*, **27**, (2008),856.

Hardebeck, J. L. and Shearer, P. M.: Using S/P amplitude ratios to constrain the focal mechanisms of small earthquakes, *Bulletin of the Seismological Society of America*, **93**, (2003), 2434–2444.

Häring, M. O., Schanz, U., Ladner, F. and Dyer, B. C.: Characterisation of the Basel 1 enhanced geothermal system, *Geothermics*, **37**, (2008), 469–495.

Ito, T. and Zoback, M. D.: Fracture permeability and in situ stress to 7 km depth in the KTB Scientific Drillhole, *Geophysical Research Letters*, **27**, (2000), 1045–1048.

Kraft, T., Wassermann, J., Schmedes, E. and Igel, H.: Meteorological triggering of earthquake swarms at Mt. Hochstaufen, SE-Germany. *Tectonophysics*, **424**, (2006), 245–258.

Moriya, H., Niitsuma, H. and Baria, R.: Multiplet-Clustering Analysis Reveals Structural Details within the Seismic. *Bulletin of the Seismological Society of America*, **93**, (2003), 1606–1620.

Mukuhira, Y., Dinske, C., Asanuma, H., Ito, T. and Häring, M. O.: Pore pressure behavior at the shut-in phase and causality of large induced seismicity at Basel, Switzerland. *Journal of Geophysical Research: Solid Earth*, **121,** (2016), 1–25.

Reasenberg, P. and Oppenheimer D.: FPFIT, FPPLOT, and FPPAGE: FORTRAN computer programs for calculating and displaying earthquake fault-plane solutions, *U.S. Geol. Surv. Open-File Rept*., (1985), 85-739.

Terakawa, T., Miller, S. A. and Deichmann, N.: High fluid pressure and triggered earthquakes in the enhanced geothermal system in Basel, Switzerland. *Journal of Geophysical Research: Solid Earth,* **117**, (2012), 1–15.

Valley, B. and Evans, K. F.: Stress orientation to 5 km depth in the basement below Basel (Switzerland) from borehole failure analysis. *Swiss Journal of Geosciences*, **102**, (2009), 467–480.

Valley, B., and Evans, K.F.: Estimation of the stress magnitude in Basel enhanced geothermal system, *Proceedings WGC 2015*, (2015).

Waldhauser, F. and Ellsworth, W. L.: A Double-difference Earthquake location algorithm: Method and application to the Northern Hayward Fault, California. *Bulletin of the Seismological Society of America*, **90**, (2000), 1353–1368.

Zoback, M.D.: Reservoir Geomechanics, Cambridge University Press, New York, NY, USA, (2007), 449.